CHEMICAL ENGINEERING TRANSACTIONS
VOL. 55, 2016
A publication of AIDIC
The Italian Association of Chemical Engineering
Online at www.aidic.it/cet
Guest Editors: Tichun Wang, Hongyang Zhang, Lei Tian

ISBN 978-88-95608-46-4; **ISSN** 2283-9216
DOI: 10.3303/CET1655048

Photocatalytic Properties of Graphene ZnNiAl-LDO Composites

Caiya Qi, Yinan Jiang, Weiwei Si, Huiyong An*

Chemical Engineering and Environmental Engineering, Liaoning Shihua University, Liaoning, China.
huianyong@163.com

In order to realize the heterogeneous phase of complex catalyst, nanoparticles immobilization and expansion application of graphene in the field of photocatalysis, through situ synthesis, graphene @ZnNiAl-LDO composite materials are produced, and with the use of XRD, FTIR, Raman, UV-vis and other characterization methods, this paper explores the differences of situ synthesis ZnNiAl-LDHs and pure ZnNiAl-LDHs structure and morphology in graphene oxide. The results show that the pure ZnNiAl-LDHs shape is micron particles in small disc. However, the situ growing ZnNiAl-LDHs in graphene oxide, its growing process is inhibited by the graphene and thus nano grain is formed. After calcination, the graphene @ZnNiAl-LDO composites were significantly improved compared with the original ZnNiAl-LDO samples in the whole UV-vis range. The absorption experiment showed that the @ZnNiAl-LDO had stronger adsorption performance of Cr(VI). Through the photocatalytic experiments, in MB and Cr (VI) coexisting solution, the visible light photocatalytic degradation rate of MB was significantly higher than that of pure MB solution, and the existence of Cr (VI) has a synergistic effect on graphene /ZnNiAl-LDO composite photocatalytic oxidation organic matter. As a result, it shows that graphene /ZnNiAl-LDO composites can be effectively used in the treatment of organic / heavy metal contaminated water.

1. Introduction

Outstanding performance of graphene and easy processing make it has a good application prospect in the field of photocatalysis and so on. Its excellent conductive properties can quickly transport photogenerated electrons, effectively separate photogenerated electrons and holes, and reduce the recombination probability.
The mixed metal oxides formed by calcination of ZnNiAl-LDHs or ZnAlTi-LDHs have excellent visible light photocatalytic activity. The contents of this paper continue to expand ZnNiAl-LDHs as the photocatalyst precursor (Compared to ZnAlTi-LDHs, the preparation of ZnNiAl-LDHs is more simple and controllable, the material yield is higher, and visible light photocatalytic activity is stronger) (Di et al., 2015). By in-situ growth method, graphene @ ZnNiAl-LDHs composite materials are synthetized. Graphite, by Hummers method oxidation and ultrasonic treatment, can be dispersed into the negatively charged graphene oxide (GO) colloid solution in water. After the GO colloidal solution is added into Zn^{2+}, Al^{3+}, Ni^{2+} and other metal ions, these metal ions can be enriched in the charged GO locus (mainly on the carboxyl group). After dynamic urea reflux, ZnNiAl-LDHs is under in-situ growth in GO, and form GO@ZnNiAl-LDHs composite materials (Hou et al., 2015). By vacuum sintering, ZnNiAl-LDHs are sintered into a mixed metal oxide, while thermal reduction of the oxidation of graphene also occurred at the same time, and ultimately form graphene @ZnNiAl-LDOs composite materials. The method is essentially to add separate GO before the preparation of LDHs, so it can get a higher yield of GO@ZnNiAl-LDHs composite materials.

2. Experiment

2.1 Experiment materials

The following components are all analytical reagent, including $Zn(NO_3)_2{\cdot}6H_2O$, $Al(NO_3)_3{\cdot}9H_2O$, $Ni(NO_3)_2{\cdot}6H_2O$, $K_2Cr_2O_7$, $CO(NH_2)_2$, HCl, and NaOH. The water used to prepare the solution and wash sample in the experiment was de ionized water.

Please cite this article as: Qi C.Y., Jiang Y.N., Si W.W., An H.Y., 2016, Photocatalytic properties of graphene znnial-ldo composites, Chemical Engineering Transactions, 55, 283-288 DOI:10.3303/CET1655048

2.2 Preparation of graphene @LDO composites

In graphene oxide @ZnNiAl-LDHs composites, the preparation of ZnNiAl-LDHs is based on the existing method of preparing ZnNiAl-LDHs for further improvement and optimization, and its hydrolysis agent is urea. The expression of the core shell structure is shown in Figure 1. The essence of in-situ growth method is to add a graphene oxide before preparing LDHs urea hydrolysis. Using graphene oxide as template, LDHs in-situ growth in graphene oxide composite materials, and form LDHs coated graphene oxide composite materials. The structure of the coated composite is similar to that of core-shell 9Gao, et al., 2015). The approximate process of preparing LDHs encapsulated graphene oxide composites by in-situ growth method is shown in Figure 2. The oxided graphene @ZnNiAl-LDHs are carried out with high temperature vacuum calcination, and finally get the product graphene @ZnNiAl-LDO photocatalyst material.

Figure 1: A schematic illustration of core-shell structure

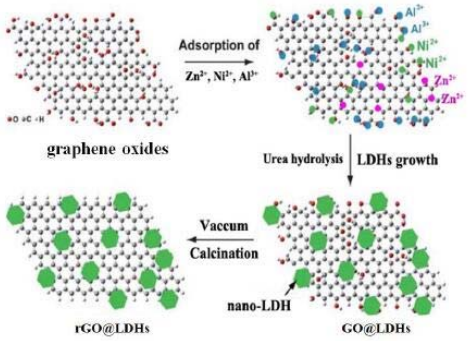

Figure 2: A schematic illustration of preparing rGO@LDO

2.3 Material characterization

(1) X-ray crystal diffraction (XRD)

The instrument of XRD powder sample used in this research is Rigaku D/MAX-IIIA. Test conditions are: Cu Kα radiation voltage for 40kV, current for 40mA, radiation wavelength for 0.154nm, the scanning speed for 17.7s/step, and 2θ scan angle range of 2-70 degrees (Liu, et al., 2015).

(2) Fourier transform infrared (FTIR) spectra

FTIR spectrum acquisition is measured by using PerkinElmer 1725 Fourier transform infrared spectrometer, KBr tablet, the deteted wave number range is 4000-400cm^{-1}, and the instrument resolution is 4cm^{-1}.

(3) Raman spectra

Raman spectra acquisition adoptsHoriba Jobin-Yvon LabRAM Raman spectrum analyser, equipped witha helium laser of 532.8nm as the excitation source, and 600 and 1200 line /mm grating, the detection range of 100-4000cm^{-1} (Zhou et al., 2015).

(4) UV-vis solid diffuse reflectance spectroscopy (DRS)

UV-vis DRS analysis uses ShimadzuUV-2450 ultraviolet spectrophotometer, equipped with an integrating sphere, with high purity barium sulfate (BaSO4) powder as a reflective substrate (Lu et al., 2016). Powder composite are evenly pressured on $BaSO_4$, and collect sample UV-vis full wavelength range (220~850nm) absorption curve.

3. Result

3.1 X- ray powder diffraction (XRD) analysis

Figure 3 shows the XRD map of GO@LDHs composites formed by LDHs with different metal ratios. The upper part of Figure 3 is the rGO@LDO composite and ZnAl-LDO formed after the GO@LDHs composite and the original ZnNiAl-LDHs are vacuum calcinated. According to the lower part of the figure, it is known that the XRD diffraction of the GO@LDHs hybrid material prepared by the in-situ growth method is basically the same as that of the original XRD diffraction, but the diffraction intensity changes (Lv et al., 2015). It is showed that the LDHs crystal structure of graphene oxide is the same as that of the original LDHs by taking oxided graphene as template. While the XRD diffraction of GO@LDHs composite is lower than that of the original LDHs, and the diffraction intensity of XRD composite is lower than that of the original.

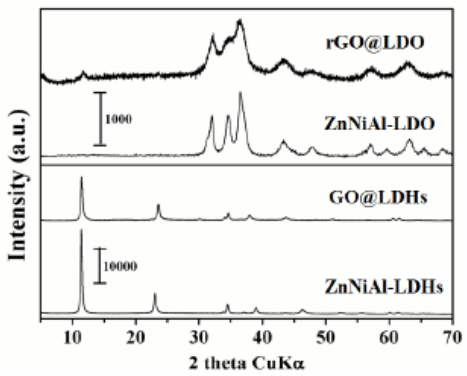

Figure 3: XRD patterns of samples

3.2 Fourier transform infrared (FTIR) spectroscopy analysis

FTIR can effectively detect the changes of the functional groups of precursors or raw materials in the preparation of rGO@LDO composites (Wang, et al., 2015). The FTIR spectra of GO, ZnNiAl-LDHs, GO@LDHs and rGO@LDO samples are shown in Figure 4. In sample GO, an absorption peak at 1730cm^{-1} can be attributed to the result of bending vibration peak of the carboxyl group on GO. However, when combined with LDHs, the carboxyl vibration peaks disappeared, which is mainly because the content of GO in the composite is low. In ZnNiAl-LDHs and GO@LDHs samples, a strong absorption peak at the 1363cm^{-1} can be attributed to the result of CO32- vibration in the ZnNiAl-CO3-LDHs itself. After vacuum calcined, rGO@LDO composites, CO32- was converted to CO2 and get out of the system so that the adsorption peak at 1363 cm^{-1} disappeared.

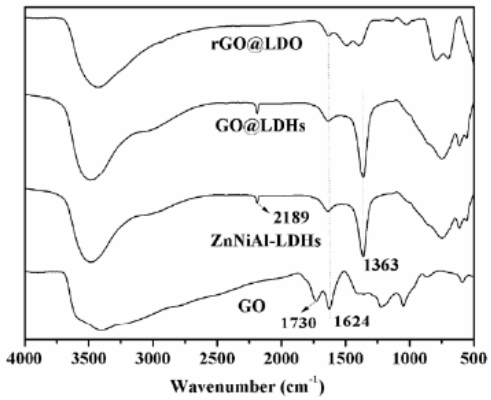

Figure 4: FTIR spectra of samples: GO, ZnNiAl-LDHs, GO@LDHs and GO@LDO

3.3 Raman spectra analysis

Carbon nano materials, because of its small dipole moment, can usually use Raman spectra or FTIR spectra to make a complementary analysis, especially the analysis of the order nature or disorder nature of the crystal structure of nano carbon materials (Wickramaratne and Jaroniec, 2015). The Raman results are shown in Figure 5.

For the Raman spectrum of nano carbon materials, it usually needs to be concerned about the two peaks of D band and G band. The signal of two peaks at 1331 and 1593cm^{-1} are respectively derived from the breathing pattern of A_{1g} symmetry point vibrational quantum of the carbon material and the first order scattering of sp^2 key E1g vibrational quantum of the carbon atom (Meksi, et al., 2016). The two peaks are denoted as D band and G band, respectively. D band and G band can be understood as the disorder of graphene and graphite carbon atoms (sp^2), respectively. For pure GO samples, the Raman signal is stronger, while the signal is obviously weakened after the composites are formed, which is mainly related to the content of GO. In the GO/LDHs and rGO/LDO composites (Uddin, et al., 2015), D band and G band can be observed, and the peak of D and G two bands can express the disorder of graphene composite materials that D/G band do, the numerical results shown in Table 1.

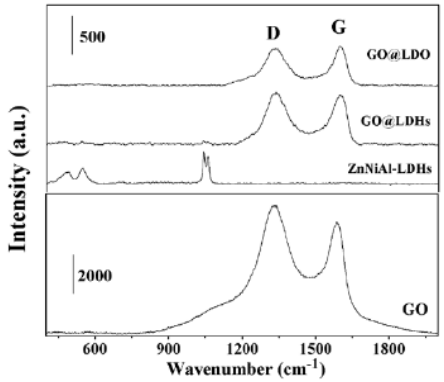

Figure 5: Raman spectra of samples: GO, ZnNiAl-LDHs, GO@LDHs and GO@LDO

Table 1. Parameters of D band and G band in the raman spectra

Sample	D band peak	G band peak	D/G band peak
GO	6414	5586	1.146
GO@LDHs	686	645	1.064
rGO@LDO	490	517	0.948

3.4 UV-vis solid diffuse reflectance spectroscopy (DRS) analysis

The UV-vis absorption curves of rGO@LDO composites and ZnAl-LDO samples are shown in Figure 6. It can be clearly observed from the graph that, the absorption value of rGO@LDO composite material is significantly improved relatively to the ZnNiAl-LDO sample in the whole UV-vis range (Mutuma, et al., 2015). It is indicated that the addition of graphene can effectively improve the absorption of ZnAl-LDO photocatalyst to UV-vis, and it provides the basis for the visible light response of rGO@LDO composites.

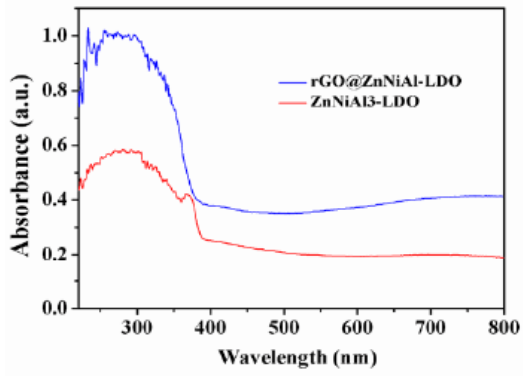

Figure 6: UV-vis absorption curves of pristine ZnNiAl-LDO and rGO@ZnNiAl-LDO

3.5 Catalytic oxidation of MB and simultaneous removal of Cr (VI)

In order to study graphene /ZnNiAl-LDO composites and at the same time carry out oxidative degradation of MB and recover the performance of Cr (VI), the effect of adsorption on the concentration of MB and Cr (VI) was investigated first of all, and the results were shown in Figure 6-9. From the built-in map in Figure 7, it can be found that MB is cationic dyes, which will be positively charged in aqueous solution, having the same charge as LDHs layers do (Perales-Martínez et al., 2015). Due to the electrostatic repulsion, LDO is not adsorbed to the MB dye. It can be observed from Figure 7 that, the absorption of ZnNiAl-LDO and rGO@LDO to Cr (VI) has reached balance in 20~30min, which is mainly caused by electrostatic attraction. Therefore, LDO has strong adsorption properties for Cr2O72- due to electrostatic attraction (Yang 2012).

For investigating the effect of Cr (VI) addition on the photocatalytic degradation of MB in graphene /ZnNiAl-LDO composites, this experiment has made a preliminary exploratory experiment (Tian et al., 2015). Prepare mixed solution containing 10mg/L MB and 10mg/L Cr (VI), add 0.5g/L graphene /ZnNiAl-LDO composites, record the MB and Cr concentration variation with time changes, and the results are shown in Figure 8 and Figure 9.

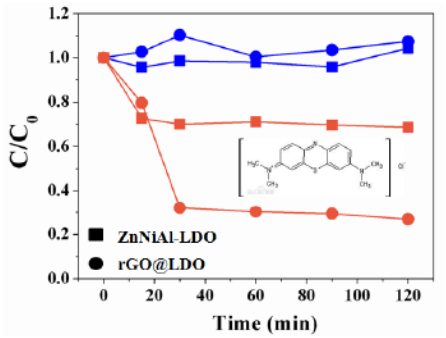

Figure 7: Adsorption of MB and Cr(IV) onto ZnNiAl-LDO and rGO@LDO. (C0(MB)=10 mg/L; C0(VI)=10 mg/L; adsorbent: 0.5g/L)

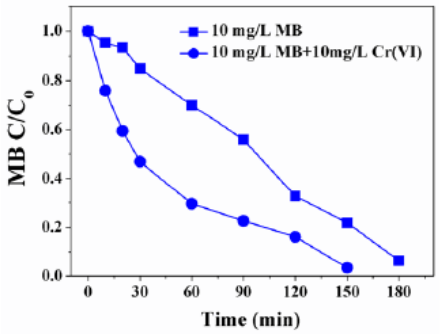

Figure 8: Effect of Cr(VI) on the photo degradation of MB by rGO@LDO. (C0(MB)=10 mg/L; C0(VI)=10 mg/L; adsorbent: 0.5g/L)

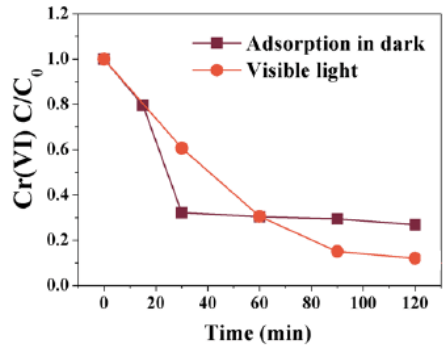

Figure 9: Cr(VI) removal during the photocatalytic reaction. (C0(MB)=10 mg/L; C0(VI)=10 mg/L; adsorbent: 0.5 g/L)

4. Conclusion

The in-situ growth method is applied to prepare graphene @ZnNiAl-LDO composite materials, and XRD, FTIR, Raman, UV-vis and other characterization methods are used to explore the differences of in-situ growth of ZnNiAl-LDHs in graphene oxide with the simple ZnNiAl-LDHs in structure and morphology. The results show that the pure ZnNiAl-LDHs is shaped in micron particles in small disc. However, ZnNiAl-LDHs with in-situ growth in graphene oxide, since the growth process is inhibited by graphene, forms the nano crystalline grain. Through the photocatalytic experiments, in MB and Cr (VI) coexisting solution, the visible light photocatalytic degradation rate of MB was significantly higher than that of pure MB solution, which suggests that Cr (VI) has a synergistic effect on graphene /ZnNiAl-LDO composite photocatalytic oxidation MB. Graphene /ZnNiAl-LDO composites can be effectively used in the treatment of organic compounds and heavy metal Cr (VI) composite contaminated water.

Acknowledgments

National Natural Science Foundation of China (Grant No. 21304042)
Natural Science Foundation of Liaoning Province of China (Grant No. 211602466)

Reference

Di J., Xia J., Ji M., Wang B., Yin S., Zhang Q., Li H., 2015, Carbon quantum dots modified BiOCl ultrathin nanosheets with enhanced molecular oxygen activation ability for broad spectrum photocatalytic properties and mechanism insight. ACS applied materials & interfaces, 7, 36, 20111-20123.

Gao W., Wang M., Ran C., Li L., 2015, Facile one-pot synthesis of MoS 2 quantum dots–graphene–TiO 2 composites for highly enhanced photocatalytic properties. Chemical Communications, 51, 9, 1709-1712.

Hou D., Hu X., Ho W., Hu P., Huang Y., 2015, Facile fabrication of porous Cr-doped SrTiO 3 nanotubes by electrospinning and their enhanced visible-light-driven photocatalytic properties. Journal of Materials Chemistry A, 3, 7, 3935-3943.

Liu T., Li Y., Zhang H., Wang M., Fei X., Duo S., Wang W., 2015, Tartaric acid assisted hydrothermal synthesis of different flower-like ZnO hierarchical architectures with tunable optical and oxygen vacancy-induced photocatalytic properties. Applied Surface Science, 357, 516-529.

Lu W., Xu T., Wang Y., Hu H., Li N., Jiang X., Chen W., 2016, Synergistic photocatalytic properties and mechanism of gC 3 N 4 coupled with zinc phthalocyanine catalyst under visible light irradiation. Applied Catalysis B: Environmental, 180, 20-28.

Lv C., Chen G., Sun J., Zhou Y., Fan S., Zhang C., 2015, Realizing nanosized interfacial contact via constructing BiVO 4/Bi 4 V 2 O 11 element-copied heterojunction nanofibres for superior photocatalytic properties.Applied Catalysis B: Environmental, 179, 54-60.

Meksi M., Turki A., Kochkar H., Bousselmi L., Guillard C., Berhault G., 2016, The role of lanthanum in the enhancement of photocatalytic properties of TiO 2 nanomaterials obtained by calcination of hydrogenotitanate nanotubes. Applied Catalysis B: Environmental, 181, 651-660.

Mutuma B.K., Shao G.N., Kim W.D., Kim H.T., 2015, Sol–gel synthesis of mesoporous anatase–brookite and anatase–brookite–rutile TiO 2 nanoparticles and their photocatalytic properties. Journal of colloid and interface science, 442, 1-7.

Perales-Martínez I.A., Rodríguez-González V., Lee S.W., Obregón S., 2015, Facile synthesis of InVO 4/TiO 2 heterojunction photocatalysts with enhanced photocatalytic properties under UV–vis irradiation. Journal of Photochemistry and Photobiology A: Chemistry, 299, 152-158.

Tian J., Leng Y., Zhao Z., Xia Y., Sang Y., Hao P., Liu H., 2015, Carbon quantum dots/hydrogenated TiO 2 nanobelt heterostructures and their broad spectrum photocatalytic properties under UV, visible, and near-infrared irradiation. Nano Energy, 11, 419-427.

Uddin M.T., Babot O., Thomas L., Olivier C., Redaelli M., D'Arienzo, Toupance T., 2015, New insights into the photocatalytic properties of RuO2/TiO2 mesoporous heterostructures for hydrogen production and organic pollutant photodecomposition. The Journal of Physical Chemistry C, 119, 13, 7006-7015.

Wang C.C., Hsueh Y.C., Su C.Y., Kei C.C., Perng T.P., 2015, Deposition of uniform Pt nanoparticles with controllable size on TiO2-based nanowires by atomic layer deposition and their photocatalytic properties.Nanotechnology, 26, 25, 254002.

Wickramaratne N.P., Jaroniec M., 2015, Ordered mesoporous carbon–titania composites and their enhanced photocatalytic properties. Journal of colloid and interface science, 449, 297-303.

Yang M., Zhang G., Wu C., Chang Z., Sun X., Duan X., 2012, Preparation of Multi-Metal Oxide Hollow Sphere Using Layered Double Hydroxide Precursors. Chinese Journal of Chemistry, 30, 9, 2183-2188.

Zhou H., Zhang H., Wang Y., Miao Y., Gu L., Jiao Z., 2015, Self-assembly and template-free synthesis of ZnO hierarchical nanostructures and their photocatalytic properties. Journal of colloid and interface science, 448, 367-373.